Low dimensional criticality embedded in high dimensional awake brain dynamics

Antonio J. Fontenele[1], J. Samuel Sooter[1], V. Kindler Norman[1], Shree Hari Gautam[1] and Woodrow L. Shew[1]

[1]Department of Physics, University of Arkansas, Fayetteville, 72701, AR, USA.

Contributing authors: shew@uark.edu;

Abstract

Cerebral cortex has been hypothesized to operate close to a critical phase transition. This hypothesis offers an explanation of the observed complexity of brain dynamics and is important because of potential computational advantages near criticality. However, in the awake state, when cortex most needs computation, experimental evidence for criticality has been inconsistent, especially when considering high precision measurements, i.e. spikes of many single neurons measured with millisecond resolution. The inconsistency of previous reports casts doubt on the possibility that awake cortex operates near criticality. Here we show that discrepant previous reports of critical phenomena in the brain may be reconciled by considering dimensionality and dimensionality reduction of brain dynamics. Indeed, fundamental physics of critical phenomena emphasizes the importance of coarse-graining of observables, which is a type of dimensionality reduction. Many detailed microscopic degrees of freedom must be excluded to reveal universal macroscopic features of criticality. We show that coarse graining over neurons and time is a type of dimensionality reduction which reveals low-dimensional critical dynamics in a prominent subspace (first few principal components) of awake cortical dynamics.

Fundamental physics of critical phenomena may govern the complex dynamics of neurons in cerebral cortex [1–3]. Experimental evidence supporting this hypothesis has come from measurements of spatiotemporal brain activity well-described by power-laws and multifaceted scaling laws predicted to occur at

criticality. The most compelling evidence, i.e. the highest quality power-laws and scaling laws, has been found when investigating *collective* brain signals, like local field potential (LFP) [4–9], wide field imaging [10, 11], and human brain imaging [7, 12]. These collective signals represent an aggregate of the underlying spike activity of many individual neurons. However, when spikes recorded in awake animals have been analyzed directly, results have been less clear - some studies report support for criticality [13–22] while others do not [6, 13, 20, 23–25]. Considering that spikes are the fundamental information carriers underlying brain function, the equivocal support for criticality at the level of spike measurements has created skepticism and confusion surrounding the hypothesis [6, 25]. Why is evidence for criticality clear in collective signals, but unclear in spike data?

A possible answer to this question is offered by basic physics of critical phenomena. Specifically, in non-living physical systems at criticality, it is necessary to coarse-grain the system observables to get beyond the detailed microscopic differences and reveal shared, universal principles. Such coarse-graining is fundamental to both theoretical understanding (e.g. the renormalization group) and experimental tests of these theories [26]. (Naively, one might suggest that everything is scale-invariant at criticality and therefore coarse-graining should not matter, but this is incorrect; at a sufficiently fine scale, scale-invariance breaks down in real systems.) Thus, it stands to reason that collective neural signals, like LFP and wide-field imaging, may reveal universal aspects of critical dynamics more reliably because they provide a macroscopic coarse-grained view of the microscopic detailed spikes; "collective" is synonymous with "coarse-grained". In this view, the inconsistency of previously reported evidence for criticality based on spikes may result from inconsistent or inadequate coarse-graining.

The plausibility of this idea is supported by a closer look at previous reports based on spike measurements in cerebral cortex of awake animals. Considering 22 experiments, a comprehensive list at the time of writing this paper (to our knowledge), 9 reported power-law avalanche statistics and the remaining 13 reported non-power-law statistics (Supplementary Table 1). The common feature of the 9 positive reports was that they performed substantial temporal coarse-graining; spike timing details at time scales below $\sim$10 ms were coarse-grained away. This temporal coarse-graining was either a deliberate step in the data analysis [13, 19] or was due to limited time resolution of experimental measurements [14, 15, 17, 20–22]. The most compelling negative reports, i.e. the worst power-laws, were based on analyses at the millisecond time scale, with little temporal coarse-graining.

Another important point of view on the effects of coarse-graining comes from many recent studies of spike activity measured in awake animals, which have shown that the activity is quite high dimensional [27–29]. By performing clever types of dimensionality reduction, specific subspaces have been revealed to be associated with specific aspects of brain function [30–34]. Moreover, many

subspaces appear to contain low amplitude fluctuations without a clear purpose. Coarse-graining is also a type of dimsionality reduction, transforming a high-dimensional detailed system down low-dimensional macroscopic variables, removing dimensions associated with microscopic details. Thus, if neural systems operate near criticality, we should seek evidence for criticality in a low-dimensional subspace and coarse-graining may be important to reveal this subspace. This idea is consistent with a recent study showing that certain subsets of neurons exhibited critical dynamics while other subsets of neurons in the same neural circuit did not [22], as well as evidence that specific neurons participate selectively in neuronal avalanches [35].

Here, we test two hypotheses: 1) criticality exists in a low-dimensional subspace, and 2) coarse-graining is essential to reveal the critical subspace. We recorded cortical neural activity in awake mice and studied a computational model. We confirmed our hypotheses showing that the critical subspace occupies a very small fraction of the full dimensionality of awake brain dynamics and that temporal coarse-graining is particularly important for revealing the critical subspace. Our results suggest that traditionally used methods often result in insufficient temporal coarse-graining, which conceals the critical subspace. As temporal coarse-graining is gradually increased, a low dimensional subspace emerges with clear critical dynamics.

1 Critical subspace

We first address the hypothesis that scale-free fluctuations may reside in a low dimensional subspace. We performed spike recordings of up to 247 units in motor cortex of awake, behaving mice (Fig. 1a, 4 mice, 19 recordings, n= 104 ± 43 single units, 44 ± 18 multi units per recording, 44 ± 9 minutes recording duration, more details in methods). Our analysis of each recording begins with generating an N $\times$ T spike count matrix (Fig. 1b, top), where N is the number of neurons and T is the number of time bins (T = recording duration divided by time bin duration ΔT). The entry in the ith row and jth column is the number of spikes fired by the ith unit during the jth time bin. We performed principal component analysis on each spike count matrix, and found that the activity is high dimensional, but much less than N dimensional; $45\% \pm 0.05$ of principal components (PCs) were needed to explain 95% of variance (Fig. 1c).

Next, we performed avalanche analysis following previously developed methods [19, 36, 37]. We created a 1-dimensional time series by summing spike counts across all N neurons and defined each avalanche as a period when this activity exceeds a threshold (Fig 1b, middle, see Methods). We found that avalanche sizes and durations were power-law distributed (purple, Fig. 1d, h) over a wide range of scales and the power-law exponents for size and duration (τ and τ_T, respectively) were related according to the crackling noise scaling law expected at criticality (Fig. 1i). Thus, we conclude that the awake spike activity we observed here is in good agreement with predictions for a system

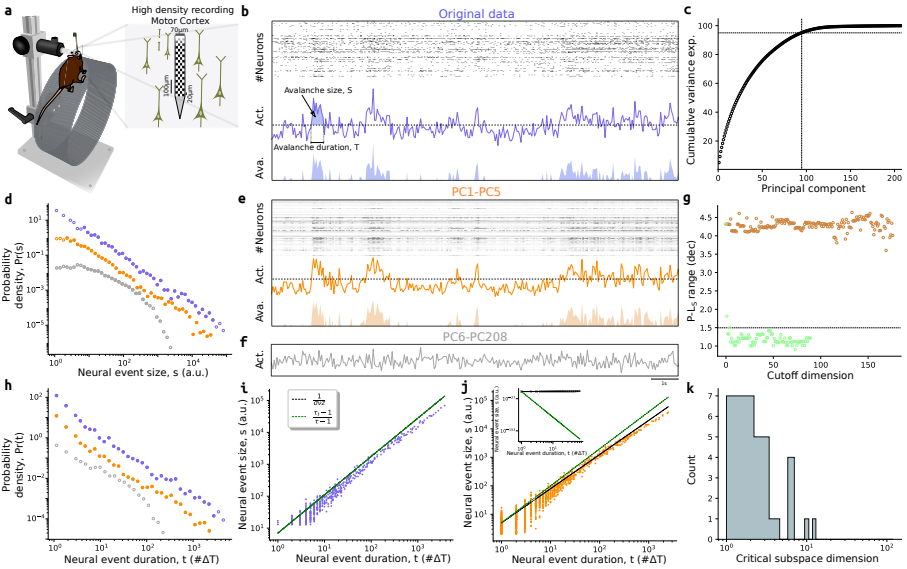

Fig. 1 Low dimensional critical subspace. a Schematic of the head-fixed preparation. The mouse is placed on top of a wheel, free to run, rest, groom, etc. High density recordings were performed in motor cortex, using a Neuropixels 1.0 probe. **b** (Top) Example raster plot for 208 units. (Middle) Spike count time series for entire population ($\Delta T = 50$ms). Dashed line represents the avalanche threshold θ. (Bottom) Avalanche time series; each shaded event represents one avalanche. **c** Cumulative variance of original activity explained by increasing number of principal components. Dashed lines marks the number of PCs needed to explain 95% of the variance. **d, h** Distributions of avalanche size (S) and duration (T) for the original data (purple), reconstructed data using the first five principal components (orange) and removing the first five components (grey). **e** Same as in **b**, but using reconstructed data based on the first five principal components. **f** Summed activity for reconstructed data based on the exclusion of the first five principal components. **g** Power-law range for avalanche size distributions as a function of PCs removed ascending/descending order (green/brown). Dimension of critical subspace is defined as the number of PCs removed before power-law range drops below 1.5 decades (dashed line). **i, j** Power-law scaling law relates size and duration of spike avalanches for original (i) and reconstructed data (j). This relation does not hold for the reconstructed data, after removing the first five components (inset). **k** Histogram of critical subspace dimension for all 19 recording sessions.

operating at criticality. (This finding depends on the choice of time scale for the time bins ΔT, which we will investigate further below.)

If these scale-free dynamics exist in a subspace then they might be robust to removal of many PCs. Initially, we tested this on the example case in Fig. 1. We generated a new N × T activity matrix, using only the first five PCs, excluding the other 203 dimensions (Methods). We found that the population spike count time series based on the reconstructed data was very similar to the original Fig. 1e. Moreover, the avalanche statistics for this 5-dimensional reconstruction remained in good agreement with predictions for criticality (orange, Fig. 1d,h,j). In contrast, if we reconstructed the data using PCs 6-208, the avalanche sizes and durations were not power-law distributed. Thus, for this

example, we conclude that the critical dynamics are primarily contained within the subspace defined by the first 5 PCs.

This example raises interesting questions. Is the dimensionality of this "critical subspace" exactly 5; is it higher or lower? Does the critical subspace always exist within the first several PCs? To address these questions, we repeated the avalanche analysis using low-dimensional reconstructed data, but systematically varying the cutoff dimension from 1 to N. For each cutoff dimension d_c ($d_c = 5$ in the example above) we performed avalanche analysis on two data sets; one reconstructed using PCs 1 through d_c, the other reconstructed using PCs $d_c + 1$ through N. For each case, we quantified the range of the avalanche size distribution that was well-fit by a power law. When reconstructed using PCs 1-d_c, the power-law range remained high, largely independent of d_c (Fig. 1g, brown). Consistent with the $d_c = 5$ example above, this suggests that the avalanche statistics are not impacted by the activity in the dimensions defined by the high PCs. Indeed, when we reconstructed the data using PCs d_c through N, the power-law range dramatically dropped when d_c exceeded a relatively small number (Fig. 1g, green). Thus, the critical subspace is highly dependent on the first few PCs. This observation suggests a convenient and quantitative definition for the dimensionality of the critical subspace - the number of PCs that can be removed (starting from PC 1) before the power-law range drops below 1.5 decades. Using this definition, we found that the critical subspace was rarely larger than 3 (10 at most, Fig. 1k). Thus, we conclude that the critical subspace is always low dimensional and is always spanned by the first few PCs.

2 Importance of coarse-graining

The activity in the critical subspace manifests as large amplitude fluctuations, coordinated across many neurons. Previous studies suggest that the spatiotemporal structure of such population activity can depend on the time scale of observation [13, 38–40]. Moreover, theory of critical phenomena suggests that temporal coarse-graining, i.e. excluding details at the small time scales, may be required to reveal universal properties of critical dynamics, as discussed above. Therefore, we next sought to determine how the critical subspace depends on the time scale of observation ΔT (for the results in Fig. 1, $\Delta T = 50$ ms). In many previous studies [6, 13, 24, 41], a common approach has been to set ΔT to the average interspike interval for the entire population of recorded neurons, following the approach pioneered by Beggs and Plenz (2003). We note, however, that this approach was originally developed for LFP events, not spikes. For our recordings here, the average spike rate across neurons was about 3 Hz. Thus, for a typical recording of 200 neurons, the interspike interval is about 1.5 ms. Obviously, this will be even smaller in cases with more recorded neurons. Here we systematically investigated a range of ΔT between 1 ms and 500 ms.

First, since the critical subspace coincides with the first several PCs, we quantified how the importance of these PCs depends on ΔT. We found that

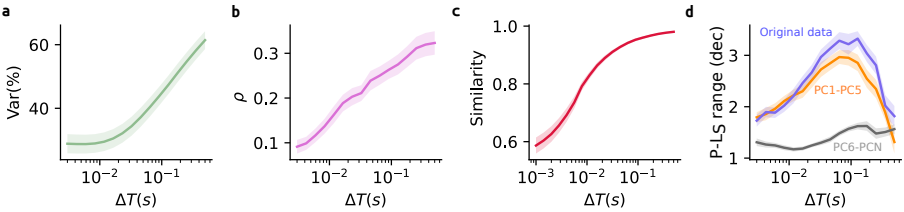

Fig. 2 Temporal coarse-graining reveals critical subspace. a, Total explained variance for the first five principal components is sensitive to temporal coarse-graining, sharply rising for $\Delta T > 10$ ms, indicating the emergence of a low-dimensional subspace. **b**, Fraction of neurons ρ engaged with (loading > 0.1) at least one of the first five principal components increases with ΔT. **c**, Similarity between the original summed population activity and that reconstructed using the first five principal components increases with ΔT. **d**, Large power-law range emerges near $\Delta T \sim 10$ ms for the original data and PCs 1-5, but not for PCs 6-N. For all panels, solid lines represent the mean across all recordings and shaded areas represents standard error.

the variance explained by the first 5 PCs is relatively small for small ΔT, but rises sharply around $\Delta T \sim 10$ ms (Fig. 2a). Next we asked how many neurons are involved in the first 5 PCs. In principle, it is possible that as few as 5 neurons are fully responsible for the first 5 PCs. We measured the fraction of neurons with strong engagement (loading > 0.1, Methods) with at least one of the first five PCs. We found that, as we increased ΔT, the fraction of neurons engaged with this low-dimensional subspace grows from 10% up to 30% (Fig. 2b); note that 30% is around 30 to 60 neurons for our recordings. Thus, the importance of the first 5 PCs is hidden for small time scales, and emerges only after temporal coarse-graining. In our initial example with $\Delta T = 50$ ms we saw that the population summed activity of the full population was very similar to that reconstructed from PCs 1-5 (Fig. 1e). Next, we asked how the similarity between these two signals depends on ΔT. We found that they were not strongly correlated for small ΔT; this correlation sharply increased around $\Delta T \sim 10$ ms (Fig. 2c). Finally, we determined how ΔT impacts the avalanche analysis on the original population summed activity and that based on PCs 1-5. We quantified the range of good power-law fit (number of decades) for the avalanche size distribution; we interpret a larger power-law range as better evidence for criticality. For both the full population and the PC 1-5 subspace, we found that at small time scales evidence for criticality is weak (power-law range is small) (Fig. 2d). The power-law range rises around $\Delta T \sim 10$ ms. If we consider avalanches based on the PC 6-N subspace, evidence for criticality is weak for all ΔT (Fig. 2d, grey). Taken together, the results in Fig. 2 show that the critical subspace will be missed if spike data are not sufficiently coarse-grained in time. The critical subspace emerges for timescales above about 10 ms.

An additional aspect of avalanche analysis that relates to coarse-graining is the choice of threshold used for defining avalanches (dashed line in Fig. 1b). A high threshold excludes many spikes from avalanches and the spikes that are excluded tend to be those that are not coordinated with the population. For example, neurons that fire asynchronously at a high rate would contribute a

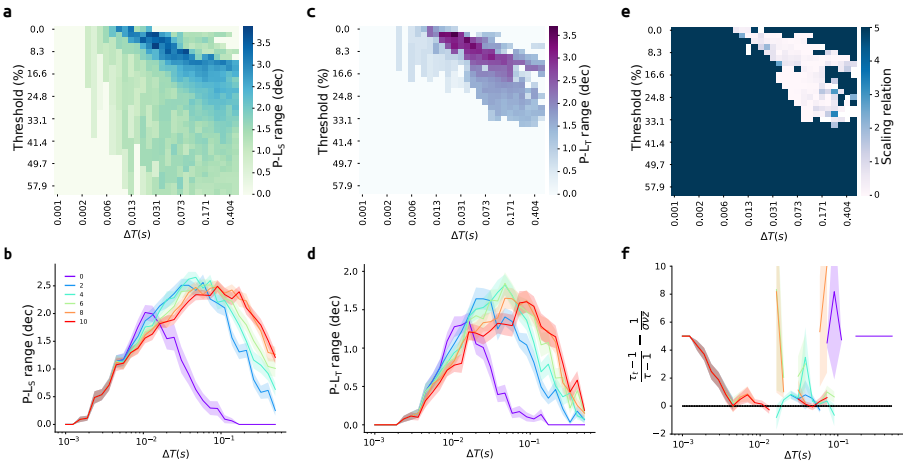

Fig. 3 Parametric study of the avalanche activity. a, single animal parametric map of power-law range of avalanche size distribution obtained for multiple thresholds (Percentile) and time bin widths (ΔT). **b**, group results for power-law range of avalanche size distribution as a function of ΔT, each curve stands for a threshold value. **c**, same as in **a** for power-law range of avalanche duration distribution. **d**, group results for power-law range of avalanche duration distribution as a function of ΔT, each curve stands for a threshold value. **e**, same as in **a** for crackling-noise scaling relation. **f**, group results for the crackling-noise scaling relation as a function of ΔT, each curve stands for a threshold value

steady, below-threshold background level to the population sum, and therefore, would not contribute to avalanches. Some previous studies have used a median threshold [22, 37], some have used the 35th percentile [19, 20], and many have used a zero threshold [6, 13, 18, 23–25, 41]. Our results in Fig. 1 and Fig. 2 are based on an 6th percentile threshold. To better understand the impact of the threshold together with temporal coarse-graining, we performed parametric avalanche analysis for a wide range of thresholds and ΔT, systematically varied from 0 to 60th percentile and from 1 ms and 500 ms, respectively. We found that for small ΔT, there was no choice of threshold that resulted in power-law avalanches (Fig. 3a-d). Above about $\Delta T \sim 10$ ms, the threshold with the largest power-law range for avalanche size grew together with ΔT; a larger threshold was needed for larger ΔT to reveal critical dynamics (Fig. 3a-d). This is consistent with previous work based on coarse-grained signals [7]. Moreover, we found that distributions of avalanche sizes and durations with large power-law range (Fig. 3a-d), as well as the crackling noise scaling law (Fig. 3e-f), emerge together at the same ΔT where the low dimensional subspace emerges Fig. 2. Thus, we conclude that the critical subspace in (Fig. 1) emerges only for sufficient temporal coarse-graining and often requires a non-zero threshold.

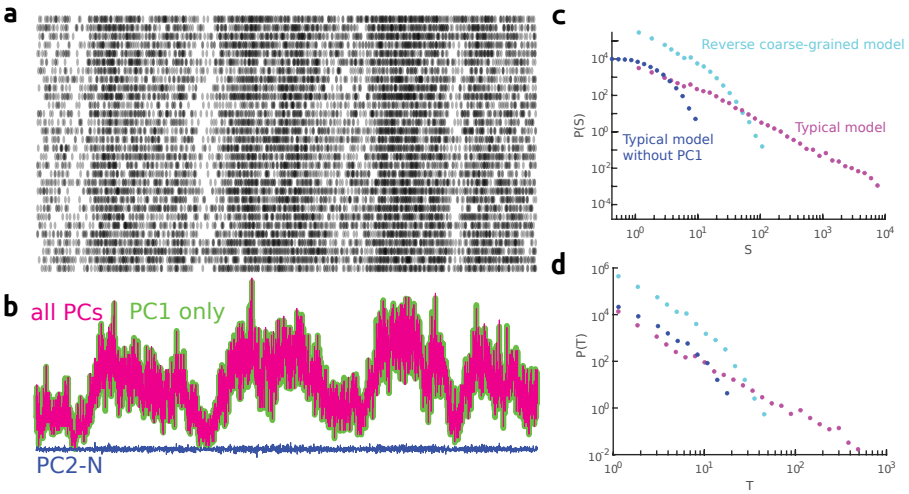

Fig. 4 Binary neuron model has one-dimensional critical subspace, matching coarse-grained experiment a, Spike raster from a subset of neurons in the model. **b**, Population sum time series is nearly identical to the PC1 time series, while remaining PCs have very weak fluctuations. **c,d**, Avalanches based on the population sum (or just PC1) have power-law distributed sizes and durations (magenta). Avalanches based on remaining PCs are not power-law distributed (blue). Reverse temporal coarse-graining abolishes power-law statistics, matching the experimental results with small ΔT (cyan).

3 Model of coarse-grained activity

How do these findings relate to computational models and theory of critical dynamics? Here we offer an answer to this question that draws upon fundamental concepts of the renormalization group [26, 42]. According to the renormalization group, simple models of critical phenomena are successful at explaining macroscopic phenomena precisely because their simplifications (compared to the real system or more complex models) exclude non-universal details that differ from one system to another. Similarly, a simple binary model of critical dynamics in neural systems has been successful at describing measurements of critical dynamics in macroscopic brain signals like LFP [8, 9, 43, 44]. Here we show in Fig. 4, that a simple binary model is successful at describing our spike recordings, but only after the experimental data are temporally coarse-grained. The model included N=1000 binary, probabilistic neurons with synaptic interactions tuned near criticality (Methods). We performed PCA on the model dynamics and found that the model is low dimensional; the first principal component alone is nearly identical to the population sum (Fig 1b). This low dimensional fluctuation exhibits critical dynamics, i.e. power-law distributed avalanche sizes and durations (Fig. 4c,d). All PCs except PC1 are devoid of critical dynamics (Fig. 4b). Thus, the model has a low-dimensional critical subspace like the experiments. However, the model matches the experiments only if the experiments are temporally coarse grained. For very small ΔT, the experimental data are high dimensional with

no power-laws not matching the model. Thus, we interpret the simple model as representing the temporally coarse-grained experiment. (Another clue which supports this interpretation is that the spike rate of model neurons matches that in the experiments only if we interpret one time step in the model as approximately 10 to 100 ms, i.e. rather coarse-grained).

If the binary model should indeed be interpreted as a model of coarse grained experimental data, then "reverse" coarse-graining the model data should abolish the power-law avalanche statistics, and better match the experiments with small ΔT. This turns out to be correct. We considered a parsimonious reverse coarse-graining scheme for the model data, which adds details at finer time scales without changing anything at coarse time scales. Before reverse coarse-graining, the model spike times are discrete, with no details at time resolutions finer than one time step. A spike that originally occurred at time step t was randomly assigned a new timestamp from the interval [t-1,t]. After such reverse coarse-graining, the model agrees well with the experiment across time scales. It produces power-law avalanches at large ΔT, but not for small ΔT.

In conclusion, we have shown that critical dynamics reside in a prominent, low-dimensional subspace of spike activity recorded from motor cortex in awake mice. This critical subspace is revealed only after sufficient coarse-graining, which may explain why some previous studies did not report critical dynamics from awake spike data. Our empirical observations match well with simple models, but only if we acknowledge that these models, by construction, represent the coarse grained experimental data, with non-universal details already excluded. Additional interesting implications of our work arise when considering the other subspaces (those orthogonal to the critical subspace). These subspaces seem to contain relatively asynchronous neural activity, compared to the large amplitude correlated fluctuations in the critical subspace. Previous work suggests that some aspects of cortical information processing are optimal near criticality, while other aspects are better suited to a more asynchronous regime [45–47]. Taken together with our results here, it may be that the computations that benefit from criticality are performed in the critical subspace, while other computations - those that benefit from an asynchronous regime - are performed outside the critical subspace. In line with this possibility, one recent study showed that subsets of neurons with critical dynamics are more strongly correlated to behavior (e.g. run speed and whisking) compared to subsets without critical dynamics [22]. Further studies are needed to explore these potential functional implications of the critical subspace and other subspaces.

4 Methods

4.1 Animals

All procedures followed the Guide for the Care and Use of Laboratory Animals of the National Institutes of Health and were approved by University of Arkansas Institutional Animal Care and Use Committee (protocol 21022). We studied adult male C57BL6/6J mice (Jackson Labs). After acclimatization to handling, a small aluminum plate (0.5 g), was attached to the skull with dental cement. Then, mice were trained for head fixation for 20 sessions, gradually increasing in duration. At the time of recordings, the mice weighed $\approx$ 28 g and were 21-23 weeks old. The 1-2 days before the first recording for each mouse, a craniotomy ($\approx$ 2 mm diameter) was performed over right motor cortex (Anterior-Posterior = 0 mm, Medial-Lateral = 1 mm). Each recording day began with a brief period of isoflurane anesthesia to expose the craniotomy and head fix the mouse. The mice were free to run, sit, groom, and walk for the entire duration (45 minutes) of each recording. During recordings, after inserting the electrode array, the craniotomy was covered with gel-foam pieces soaked in sterile phosphate buffer solution.

4.2 Electrophysiology

The extracellular voltage was recorded using Neuropixels probes (NP version 1.0, IMEC) consisting of an electrode shank (width: 70 μm, length: 10 mm, thickness: 100 µm) of 960 total sites laid out in a checkerboard pattern with contacts at $\approx$18-μm site-to-site distances (16 μm (column), 20 μm (row)), enabling up to 384 recording channels. On the recording day, following head fixation, the Neuropixels probe was inserted to a tip-depth of approximately 1.2 mm, ensuring that the active recording sites spanned all cortical layers. A Ag/AgCl pellet was used as ground, placed in the saline-soaked gel foam covering the craniotomy. The ground pellet wire was soldered to the Neuropixel midway along the ribbon cable. Electrophysiological data were collected (30 kHz) using SpikeGLX software. Spike sorting was performed using Kilosort 3.0 (https://github.com/MouseLand/Kilosort) and then manually curated using phy (https://github.com/cortex-lab/phy) [48].

4.3 Data analysis

4.3.1 PCA

To generate results presented in Figs. 1 and 2, we performed principal component analysis (PCA) in Python using the function **decomposition.PCA** from package sklearn. Let $\mathbf{Z}$ be a spike count matrix with T rows (number of time bins) and N columns (number of neurons). Then, PCA generates $\mathbf{V}$ which contains the eigenvectors of the covariance matrix of $\mathbf{Z}$. $\mathbf{V}$ has N rows and N columns (one column for each eigenvector, i.e. one column for each principal component). We calculated % variance explained by a set of PCs as the sum

of their corresponding eigenvalues of $\mathbf{V}$ (reported in Fig. 1c and Fig. 2a). To reconstruct data based on a subset of PCs (e.g. PCs 1-K), we first define the PCA projection matrix by $\mathbf{B} = \mathbf{ZV}$, which results in a $T \times K$ matrix. Then to reconstruct N dimensional data $\hat{\mathbf{Z}}$, we multiply $\hat{\mathbf{Z}} = \mathbf{BV}^T = \mathbf{ZVV}^T$.

4.3.2 Avalanche analysis

The first step in avalanche analysis was to create a spike count matrix $\mathbf{Z}$; Z_{tj} is the number of spikes fired by unit j during time bin t. Next, the population sum spike count time series X was created by summing spike counts over all neurons at each time bin, $X_t = \sum_j Z_{tj}$. The threshold θ used for avalanche detection was defined as some percentile (0 to 60th were considered) of X. By definition, an avalanche begins when X exceeds the threshold and ends when X returns below threshold. The size S of an avalanche is defined as $S = \sum_{t_i}^{t_f}(X_t - \theta)$, where the start and end times of the avalanche are t_i and t_f, respectively. Avalanche duration is defined as $T = t_f - t_i$.

In order to assess whether avalanche sizes and durations were distributed according to a power-law and to obtain power-law exponents and ranges, we built on previously developed maximum likelihood methods [8, 22, 49, 50]. In brief, the fitting algorithm identifies the best fit truncated power-law that meets a pre-defined goodness-of-fit criterion. There are three fitting parameters: the minimum avalanche size x_m, the maximum avalanche size x_M, and the power-law exponent τ. The following steps summarize the algorithm. First, outliers were excluded. Second, events with size/duration less than x_m and larger than x_M were excluded. Third, the maximum likelihood power-law exponent was calculated. Fourth, we assessed the goodness-of-fit. We repeated these four steps for all the possible pairs of x_m and x_M values, in the end, identifying the largest power-law range that passed our goodness-of-fit criterion. We define power-law range as the number of decades of power-law scaling $\log_{10}\frac{x_M}{x_m}$. We note that this algorithm is independent of any choice of bins used to create the PDF plots in the paper.

The primary improvement we made compared to our most recently published methods [22] was to make our goodness-of-fit criterion less sensitive to sample size (number of avalanches) and more computationally efficient. For a given x_m, x_M, and τ, goodness-of-fit was quantified as follows. First, we created a cumulative distribution function (CDF) of the real data (excluding samples below x_m or above x_M). Second, we define a theoretical CDF for a truncated power-law with the same range and exponent: for both discrete variables $P(x \leq s) = \frac{\sum_{x=x_m}^{s} x^{-\tau}}{\sum_{x=x_m}^{x_M} x^{-\tau}}$ and continuous variables $P(x \leq s) = \frac{x^{-\tau+1} - x_m^{-\tau+1}}{x_M^{-\tau+1} - x_m^{-\tau+1}}$. Third, we define a region delimited by upper and lower bounds defined as the theoretical CDF +0.03 and -0.03, respectively. Fourth, we resample the real CDF at 10 logarithmically spaced values per decade. Fifth, we calculated the fraction F of resampled points in the CDF of the real data that fell within ± 0.03 bounds of the theoretical CDF. F is our goodness-of-fit measure. F=1

means that the entire range of the real data varies less than 3% from a perfect power-law. We sought the fit with largest power-law range that meets the goodness-of-fit criterion $F \geq 0.85$.

4.4 Computational model

The model consists of 1000 excitatory units. As discussed above, we interpret each unit as a temporally coarse-grained neuron. The units are interconnected randomly and sparsely (Erdos-Renyi, 90% of connections set to zero). A neuron spikes at time step t with probability

$$P_i(t) = \eta + \sum_j W_{ij} S_j(t-1)$$

where $\eta = 0.003$ is a baseline spiking probability, W is the connectivity matrix, and

$$S_j(t) = \begin{cases} 1 & \text{if the } j\text{th neuron spikes at time step } t \\ 0 & \text{otherwise} \end{cases}$$

All non-zero entries of W are equal to the same constant. We tuned the model close to criticality by multiplying W by a constant resulting in the magnitude of the largest eigenvalue of W set to 0.99. For the avalanche analysis in Fig. 4, we considered a random subsample of 150 units to match the typical number of neurons in our experimental recordings. To implement "reverse" coarse-graining, we assigned each spike a time chosen at random from the interval $[(t-1), t]$, where t is the time step at which the spike occurred. The result is a two-column matrix; one column for spike times and the other for unit identities. This data was analyzed in the same way as the spike-sorted experimental data.

Supplementary information

Authors	Journal	Year	Orgaanism	Measurement device	Time bin duration (ms)	Avalanche threshold (%)	high density	Temporal resolution (ms)
Ponce-Alvarez et al	Neuron	2018	zebra fish	2p Ca imaging	470	n/a	X	470
Jones et al	biorXiv	2022	mouse	2p Ca imaging	300	50	X	300
Karimipanah et al	Plos One	2017	mouse	2p Ca imaging	250	50	X	250
Curic et al	J Phys Complexity	2021	mouse	2p Ca imaging	50	0*	X	50
Ma et al	Neuron	2019	mouse	16 ch array	40	35	X	<1
Ma et al	J Neurophys	2020	mouse	2p Ca imaging	30	35	X	30
Bowen et al	Frontiers Sys Neuro	2019	mouse	2p Ca imaging	30	0*	X	30
Bellay et al	eLife	2015	mouse	2p Ca imaging	30	0*	X	30
Hahn et al	Plos Comp Biol	2017	monkey	96 ch MEA (utah)	14 - 31	0		<1
Priesemann et al	Frontiers Sys Neuro	2014	rat	32 or 64 ch Buzsaki probes	16	0	X	<1
			cat	54 ch polytrodes	16	0	X	<1
			monkeys	16 single wires (4x4 grid)	16	0		<1
Dehghani et al	Frontiers Physiol	2012	cat	96 ch MEA (utah)	1 - 16	0		<1
			monkey	96 ch MEA (utah)	1 - 16	0		<1
			humans	96 ch MEA (utah)	1 - 16	0		<1
Ribiero et al	Plos One	2010	rat	16-32 ch micro wire	1 - 20	0		<1
Fontenele et al	Phys Rev Lett	2019	mouse	64 ch array	3	0	X	<1
Priesemann et al	Frontiers Sys Neuro	2014	rat	32 or 64 ch Buzsaki probes	0.5	0	X	<1
			cat	54 ch polytrodes	0.5	0	X	<1
			monkeys	16 single wires (4x4 grid)	0.5	0		<1
Touboul & Destexhe	Plos One	2010	cat	MEA (8 ch)	n/r	0		<1
Bedard & Destexhe	Phys Rev Lett	2006	cat	MEA (8 ch)	n/r	0		<1

Table S1. Discrepancies among previous reports of spike avalanches in awake animals may be explained by insufficient temporal coarse-graining. Tabulated details from previous experiments, limited to cases in awake animals with single neuron resolution. White background color indicates studies that reported support for criticality based on spike avalanches distributed according to power-laws. Yellow background color indicates studies that reported evidence against criticaltiy, i.e. poor avalanche power laws. Rows are ordered top to bottom according to the time bin duration ΔT of avalanche analysis. The fact that the top rows (with one exception) reported power-laws implicates the importance of temporal coarse-graining for revealing critical dynamics. Fontenele et al (2019) was marked orange because they analyzed how avalanches change over time during long recordings and found that the vast majority of time in the awake state was not in agreement with scaling laws found at criticality. This summary also agrees with our finding that avalanche threshold needs to be larger for larger ΔT to find criticality. We note that the studies marked 0* in the threshold column are a special case. They employed a type of deconvolution of Ca fluorescence signals to recover spike probability. They chose a threshold in the deconvolution process that resulted in maximum number of avalanches. This is difficult to compare with the percentile threshold we studied here, but is similar to choosing a non-zero, intermediate percentile. Finally, we note that in addition to the time scale ΔT, the spatial density of the recorded neurons also seems to be correlated with whether avalanches were reported as power-laws or not (column labeled "high

density"). This could also be an important factor. For example, the one case that is not well explained by time bin duration (Hahn et al, 2017) was based on low density measurements - typical distance between any pair of neurons is more than 400 microns for Utah array recordings.

References

[1] Muñoz, M.A.: Colloquium: Criticality and dynamical scaling in living systems. Reviews of Modern Physics **90**(3), 31001 (2018) arXiv:1712.04499. https://doi.org/10.1093/ejcts/ezx068

[2] Beggs, J.M.: The Cortex and the Critical Point. MIT Press, Cambridge, MA (2022)

[3] O'Byrne, J., Jerbi, K.: How critical is brain criticality? Trends in Neurosciences **45**(11), 820–837 (2022). https://doi.org/10.1016/j.tins.2022.08.007

[4] Beggs, J.M., Plenz, D.: Neuronal avalanches in neocortical circuits. Journal of Neuroscience **23**(35), 11167–77 (2003)

[5] Klaus, A., Yu, S., Plenz, D.: Statistical analyses support power law distributions found in neuronal avalanches. PloS one **6**(5), 19779 (2011). https://doi.org/10.1371/journal.pone.0019779

[6] Dehghani, N., Hatsopoulos, N.G., Haga, Z.D., Parker, R.a., Greger, B., Halgren, E., Cash, S.S., Destexhe, A.: Avalanche Analysis from Multielectrode Ensemble Recordings in Cat, Monkey, and Human Cerebral Cortex during Wakefulness and Sleep. Frontiers in physiology **3**(August), 302 (2012). https://doi.org/10.3389/fphys.2012.00302

[7] Zhigalov, A., Arnulfo, G., Nobili, L., Palva, S., Palva, J.M.: Relationship of Fast- and Slow-Timescale Neuronal Dynamics in Human MEG and SEEG. Journal of Neuroscience **35**(13), 5385–5396 (2015). https://doi.org/10.1523/JNEUROSCI.4880-14.2015

[8] Shew, W.L., Clawson, W.P., Pobst, J., Karimipanah, Y., Wright, N.C., Wessel, R.: Adaptation to sensory input tunes visual cortex to criticality. Nature Physics, 1–48 (2015). https://doi.org/10.1038/nphys3370

[9] Yu, S., Ribeiro, T.L., Meisel, C., Chou, S., Mitz, A., Saunders, R., Plenz, D.: Maintained avalanche dynamics during task-induced changes of neuronal activity in nonhuman primates. eLife **6** (2017). https://doi.org/10.7554/eLife.27119

[10] Scott, G., Fagerholm, E.D., Mutoh, H., Leech, R., Sharp, D.J.,

Shew, W.L., Knopfel, T.: Voltage Imaging of Waking Mouse Cortex Reveals Emergence of Critical Neuronal Dynamics. Journal of Neuroscience **34**(50), 16611–16620 (2014). https://doi.org/10.1523/JNEUROSCI.3474-14.2014

[11] Fagerholm, E.D., Scott, G., Shew, W.L., Song, C., Leech, R., Knöpfel, T., Sharp, D.J.: Cortical Entropy, Mutual Information and Scale-Free Dynamics in Waking Mice. Cerebral Cortex, 1–8 (2016). https://doi.org/10.1093/cercor/bhw200

[12] Tagliazucchi, E., Balenzuela, P., Fraiman, D., Chialvo, D.R.: Criticality in large-scale brain FMRI dynamics unveiled by a novel point process analysis. Frontiers in physiology **3**(February), 15 (2012). https://doi.org/10.3389/fphys.2012.00015

[13] Priesemann, V., Wibral, M., Valderrama, M., Pröpper, R., Le Van Quyen, M., Geisel, T., Triesch, J., Nikolić, D., Munk, M.H.J.: Spike avalanches in vivo suggest a driven, slightly subcritical brain state. Frontiers in systems neuroscience **8**(June), 108 (2014). https://doi.org/10.3389/fnsys.2014.00108

[14] Bellay, T., Klaus, A., Seshadri, S., Plenz, D.: Irregular spiking of pyramidal neurons organizes as scale-invariant neuronal avalanches in the awake state. eLife **4**, 1–25 (2015). https://doi.org/10.7554/eLife.07224

[15] Karimipanah, Y., Ma, Z., Miller, J.-E.K., Yuste, R., Wessel, R.: Neocortical activity is stimulus- and scale-invariant. PloS one **12**(5), 0177396 (2017). https://doi.org/10.1371/journal.pone.0177396

[16] Ponce-Alvarez, A., Jouary, A., Privat, M., Deco, G., Sumbre, G.: Whole-Brain Neuronal Activity Displays Crackling Noise Dynamics. Neuron **100**(6), 1446–14596 (2018). https://doi.org/10.1016/j.neuron.2018.10.045

[17] Bowen, Z., Winkowski, D.E., Seshadri, S., Plenz, D., Kanold, P.O.: Neuronal Avalanches in Input and Associative Layers of Auditory Cortex. Frontiers in Systems Neuroscience **13** (2019). https://doi.org/10.3389/fnsys.2019.00045

[18] Fontenele, A.J., De Vasconcelos, N.A.P., Feliciano, T., Aguiar, L.A.A., Soares-Cunha, C., Coimbra, B., Dalla Porta, L., Ribeiro, S., Rodrigues, A.J., Sousa, N., Carelli, P.V., Copelli, M.: Criticality between Cortical States. Physical Review Letters **122**(20), 208101 (2019). https://doi.org/10.1103/PhysRevLett.122.208101

[19] Ma, Z., Turrigiano, G.G., Wessel, R., Hengen, K.B.: Cortical Circuit Dynamics Are Homeostatically Tuned to Criticality In Vivo. Neuron

104(4), 655–6644 (2019). https://doi.org/10.1016/j.neuron.2019.08.031

[20] Ma, Z., Liu, H., Komiyama, T., Wessel, R.: Stability of motor cortex network states during learning-associated neural reorganizations. Journal of Neurophysiology **124**(5), 1327–1342 (2020). https://doi.org/10.1152/jn.00061.2020

[21] Curic, D., Ivan, V.E., Cuesta, D.T., Esteves, I.M., Mohajerani, M.H., Gruber, A.J., Davidsen, J.: Deconstructing scale-free neuronal avalanches: behavioral transitions and neuronal response. Journal of Physics: Complexity **2**(4), 045010 (2021). https://doi.org/10.1088/2632-072X/ac35b4

[22] Jones, S.A., Barfield, J.H., Kindler Norman, V., Shew, W.L.: Scale-free behavioral dynamics directly linked with scale-free cortical dynamics. bioRxiv (2022). https://doi.org/10.1101/2021.05.12.443799

[23] Bédard, C., Kröger, H., Destexhe, A.: Does the 1/f frequency scaling of brain signals reflect self-organized critical states? Physical Review Letters **97**(11), 1–4 (2006) arXiv:0608026 [q-bio]. https://doi.org/10.1103/PhysRevLett.97.118102

[24] Ribeiro, T.L., Copelli, M., Caixeta, F., Belchior, H., Chialvo, D.R., Nicolelis, M.a.L., Ribeiro, S.: Spike avalanches exhibit universal dynamics across the sleep-wake cycle. PloS one **5**(11), 14129 (2010). https://doi.org/10.1371/journal.pone.0014129

[25] Touboul, J., Destexhe, A.: Can power-law scaling and neuronal avalanches arise from stochastic dynamics? PloS one **5**(2), 8982 (2010). https://doi.org/10.1371/journal.pone.0008982

[26] Stanley, H.E.: Scaling, universality, and renormalization: Three pillars of modern critical phenomena. Rev. Mod. Phys. **71**(2), 358 (1999)

[27] Gao, P., Trautmann, E., Yu, B., Santhanam, G., Ryu, S., Shenoy, K., Ganguli, S.: A theory of multineuronal dimensionality, dynamics and measurement. bioRxiv (2017). https://doi.org/10.1101/214262

[28] Stringer, C., Pachitariu, M., Steinmetz, N., Reddy, C.B., Carandini, M., Harris, K.D.: Spontaneous behaviors drive multidimensional, brainwide activity. Science **364**(6437), 7893 (2019). https://doi.org/10.1126/science.aav7893

[29] Umakantha, A., Morina, R., Cowley, B.R., Snyder, A.C., Smith, M.A., Yu, B.M.: Bridging neuronal correlations and dimensionality reduction. Neuron **109**(17), 2740–275412 (2021). https://doi.org/10.1016/j.neuron.2021.06.028

[30] Semedo, J.D., Zandvakili, A., Machens, C.K., Yu, B.M., Kohn, A.: Cortical Areas Interact through a Communication Subspace. Neuron **102**(1), 249–2594 (2019). https://doi.org/10.1016/j.neuron.2019.01.026

[31] Tang, C., Herikstad, R., Parthasarathy, A., Libedinsky, C., Yen, S.C.: Minimally dependent activity subspaces for working memory and motor preparation in the lateral prefrontal cortex. eLife **9**, 1–23 (2020). https://doi.org/10.7554/ELIFE.58154

[32] Li, J., Kells, P.A., Osgood, A.C., Gautam, S.H., Shew, W.L.: Collapse of complexity of brain and body activity due to excessive inhibition and MeCP2 disruption. Proceedings of the National Academy of Sciences **118**(43), 2106378118 (2021). https://doi.org/10.1073/pnas.2106378118

[33] Flesch, T., Juechems, K., Dumbalska, T., Saxe, A., Summerfield, C.: Orthogonal representations for robust context-dependent task performance in brains and neural networks. Neuron **110**(7), 1258–127011 (2022). https://doi.org/10.1016/j.neuron.2022.01.005

[34] Barreiro, A.K., Ly, C., Raju, P., Gautam, S.H., Shew, W.L.: Sensory input to cortex encoded on low-dimensional periphery-correlated subspaces. bioRxiv (2022). https://doi.org/10.1101/2022.06.15.496327

[35] Bellay, T., Shew, W.L., Yu, S., Falco-Walter, J.J., Plenz, D.: Selective Participation of Single Cortical Neurons in Neuronal Avalanches. Frontiers in Neural Circuits **14**(301), 1–18 (2021). https://doi.org/10.3389/fncir.2020.620052

[36] Poil, S.-S., Hardstone, R., Mansvelder, H.D., Linkenkaer-Hansen, K.: Critical-state dynamics of avalanches and oscillations jointly emerge from balanced excitation/inhibition in neuronal networks. Journal of Neuroscience **32**(29), 9817–23 (2012). https://doi.org/10.1523/JNEUROSCI.5990-11.2012

[37] Gautam, S.H., Hoang, T.T., McClanahan, K., Grady, S.K., Shew, W.L.: Maximizing Sensory Dynamic Range by Tuning the Cortical State to Criticality. PLOS Computational Biology **11**(12), 1004576 (2015). https://doi.org/10.1371/journal.pcbi.1004576

[38] Leopold, D.A., Murayama, Y., Logothetis, N.K.: Very slow activity fluctuations in monkey visual cortex: implications for functional brain imaging. Cerebral Cortex **13**(4), 422 (2003)

[39] Doiron, B., Litwin-Kumar, A., Rosenbaum, R., Ocker, G.K., Josić, K.: The mechanics of state-dependent neural correlations. Nature Neuroscience **19**(3), 383–393 (2016). https://doi.org/10.1038/nn.4242

[40] Okun, M., Steinmetz, N.A., Lak, A., Dervinis, M., Harris, K.D.: Distinct Structure of Cortical Population Activity on Fast and Infraslow Timescales. Cerebral Cortex **29**, 2196–2210 (2019). https://doi.org/10.1093/cercor/bhz023

[41] Hahn, G., Ponce-Alvarez, A., Monier, C., Benvenuti, G., Kumar, A., Chavane, F., Deco, G., Frégnac, Y.: Spontaneous cortical activity is transiently poised close to criticality. PLOS Computational Biology **13**(5), 1005543 (2017). https://doi.org/10.1371/journal.pcbi.1005543

[42] Sethna, J.P., Dahmen, K.a., Myers, C.R.: Crackling noise. Nature **410**(6825), 242–50 (2001). https://doi.org/10.1038/35065675

[43] Poil, S.-S., van Ooyen, A., Linkenkaer-Hansen, K.: Avalanche dynamics of human brain oscillations: relation to critical branching processes and temporal correlations. Human brain mapping **29**(7), 770–7 (2008). https://doi.org/10.1002/hbm.20590

[44] Shew, W.L., Yang, H., Petermann, T., Roy, R., Plenz, D.: Neuronal Avalanches Imply Maximum Dynamic Range in Cortical Networks at Criticality. Journal of Neuroscience **29**(49), 15595–15600 (2009). https://doi.org/10.1523/JNEUROSCI.3864-09.2009

[45] Tomen, N., Rotermund, D., Ernst, U.: Marginally subcritical dynamics explain enhanced stimulus discriminability under attention. Frontiers in Systems Neuroscience **8**(August), 1–15 (2014). https://doi.org/10.3389/fnsys.2014.00151

[46] Clawson, W.P., Wright, N.C., Wessel, R., Shew, W.L.: Adaptation towards scale-free dynamics improves cortical stimulus discrimination at the cost of reduced detection. PLOS Computational Biology **13**(5), 1005574 (2017). https://doi.org/10.1371/journal.pcbi.1005574

[47] Wilting, J., Dehning, J., Pinheiro Neto, J., Rudelt, L., Wibral, M., Zierenberg, J., Priesemann, V.: Operating in a reverberating regime enables rapid tuning of network states to task requirements. Frontiers in Systems Neuroscience **12**, 55 (2018)

[48] Pachitariu, M., Steinmetz, N., Kadir, S., Carandini, M., Harris, K.D.: Kilosort: realtime spike-sorting for extracellular electrophysiology with hundreds of channels. bioRxiv, 061481 (2016). https://doi.org/10.1101/061481

[49] Clauset, A., Shalizi, C.R., Newman, M.E.J.: Power-Law Distributions in Empirical Data. SIAM Review **51**(4), 661–703 (2009) arXiv:arXiv:0706.1062v2. https://doi.org/10.1137/070710111

[50] Langlois, D., Cousineau, D., Thivierge, J.P.: Maximum likelihood estimators for truncated and censored power-law distributions show how neuronal avalanches may be misevaluated. Physical Review E **89**(1), 012709 (2014). https://doi.org/10.1103/PhysRevE.89.012709